Experimental and numerical investigation of residual stresses in laser shock peened AA2198

Keller, S.; Chupakhin, S.; Staron, P.; Maawad, E.; Kashaev, N.; Klusemann, B.

Published in:
Journal of Materials Processing Technology

DOI:
10.1016/j.jmatprotec.2017.11.023

Publication date:
2018

Document Version
Publisher's PDF, also known as Version of record

Journal of Materials Processing Tech. 255 (2018) 294–307

Contents lists available at ScienceDirect

Journal of Materials Processing Tech.

journal homepage: www.elsevier.com/locate/jmatprotec

Experimental and numerical investigation of residual stresses in laser shock peened AA2198

S. Keller[a,*], S. Chupakhin[a], P. Staron[a], E. Maawad[a], N. Kashaev[a], B. Klusemann[a,b]

[a] Helmholtz-Zentrum Geesthacht, Institute of Materials Research, Materials Mechanics, Max-Planck-Straße 1, 21052 Geesthacht, Germany
[b] Leuphana University of Lüneburg, Institute of Product and Process Innovation, Volgershall 1, 21339 Lüneburg, Germany

ARTICLE INFO

Keywords:
Laser shock peening
AA2198
Residual stress
Hole drilling
X-ray diffraction
Focus size
Tempering conditions
Finite element analysis

ABSTRACT

Laser shock peening (LSP) is a surface treatment which improves the fatigue performance of metallic structures by introducing compressive residual stresses. The aim of this paper is the investigation of LSP of the aluminium alloy AA2198. This investigation includes the variation of the laser power density (2.78–25 GW/cm^2) and the square laser focus (1 mm × 1 mm and 3 mm × 3 mm). Additionally, two different temper stages (T3 and T8) and thicknesses (3.2 mm and 4.8 mm) of AA2198 are considered. The study of the LSP process is split into two parts; at first, LSP experiments are performed to clarify the influence of the temper stage, the focus size, the laser power density and the thickness of the specimen on the residual stress field. Secondly, a process model based on the finite element method is employed which requires in particular the adjustment of a suitable laser induced pressure pulse. Due to the different yield strength and strain hardening behaviour of the different temper conditions, AA2198-T8 shows a lower penetration depth of compressive residual stresses compared to AA2198-T3. A smaller focus size leads to higher compressive residual stresses near the surface but a lower penetration depth. To investigate possible shock wave reflections, different base layers in the LSP process are investigated considering a free, a clamped and a glued back-side of the specimen. No differences in terms of resulting residual stresses were observed. The experimental study provides some preliminary assumptions which are used to simplify the simulation set-up. Residual stresses are measured by the incremental hole drilling method using electronic speckle pattern interferometry (ESPI) as well as synchrotron X-ray diffraction. The calculated residual stresses in the simulation are averaged layer-wise over a sample area for comparison with the measured residual stresses. The model is used to simulate the LSP process for the considered temper stages and focus sizes to predict the resulting residual stresses. Simulated and measured residual stress profiles show for the different cases very good agreement.

1. Introduction

Laser shock peening (LSP) is a contact-free surface enhancement technique. Peyre et al. (1996) showed the improved fatigue performance on the cycle properties of different aluminium alloys. Clauer and Lahrman (2001) provided an overview of the surface enhancement properties achievable by LSP such as an increased corrosion resistance of the aluminium alloy AA2024-T3, which is investigated by Clauer et al. (1977). Handling fatigue and corrosion failure causes in light weight structures are main challenges in the aerospace industry as documented by Reid (2003). The aim of LSP is to generate compressive residual stresses in critical regions of fatigue. Crack driving tensile stresses have to overcome these compressive stresses to cause failure of the structure. Hence, addition of compressive residual stresses on possible tensile stresses caused by service loads leads to an increased fatigue life.

After the discovery of the effect of laser beam pulses on a target (Askar'yan and Moroz, 1963) followed by early publications (Fairand et al., 1972) which are focused on the microstructural and mechanical property changes in the material, LSP has been investigated continuously. This work contains the investigation of the LSP process of thin sheets consisting of AA2198 using an high energy laser enabling a laser power density up to 25 GW/cm^2. Dursun and Soutis (2014) provided recently a review on developments in advanced aircraft aluminium alloys. AA2198 is an aluminium-lithium alloy of the third generation and were developed for the aircraft industry to substitute common used aluminium-copper alloys such as AA2024. The advantage over traditionally used procedures (e.g. shot peening) is a higher penetration depth (in mm range) of compressive stresses in conjunction with a high surface quality (Peyre et al., 1996). Additionally, LSP allows

* Corresponding author.
E-mail address: soeren.keller@hzg.de (S. Keller).

https://doi.org/10.1016/j.jmatprotec.2017.11.023
Received 7 February 2017; Received in revised form 18 September 2017; Accepted 16 November 2017
Available online 20 November 2017

to treat complex geometries and does not involve any direct physical contact. A main difficulty in LSP are the many process parameters which influence the resulting residual stress field. Hence, experimental based optimization of LSP is a time consuming process.

Therefore, numerical simulation of LSP can speed up optimization processes and help understanding mechanisms which are difficult to measure (e.g. shock wave propagation). The first finite element (FE) simulation of LSP has been reported by Braisted and Brockman (1999). Depending on the specific research question of the simulation (e.g. prediction of the residual stresses, wave propagation or fatigue behaviour) several LSP process models based on the FE method were developed. Especially the discretised geometry and related simplifications (e.g. the use of symmetry conditions) influences the numerical effort. Using the rotational symmetry of circular laser spots two-dimensional FE models are resource effective tools to predict residual stresses. Thus, Ding and Ye (2006) used a two-dimensional-axisymmetric FE model which was in reasonable agreement to experimental data. The authors investigated the laser focus size and the influence of overlap, i.e. multiple laser pulses at the same spot. Sticchi et al. (2015) compared results of two-dimensional-axisymmetric and three dimensional FE model for LSP with overlap. It was concluded, that the fast and simple two-dimensional model can be used for first estimations. Three-dimensional models simulating a half space of the material using infinite elements were used to calculate detailed residual stress fields of pressure pulse-material configurations which the two-dimensional approach did not allow (e.g. square laser focus, specific laser pulse sequences or anisotropic material properties). Ocana et al. (2004) simulated deformations and residual stresses with a three-dimensional semi-infinite FE model. It is stated that a three-dimensional treatment of the LSP process is necessary for an effective assessment of the LSP technology. The use of an semi-infinite three-dimensional model is effective to determine the influence of the LSP conditions and material properties on the residual stress field but do not consider the specific geometry of a component. Three-dimensional discretisations of the whole component (Bhamare et al., 2013) or a part of it (Spradlin et al., 2011) lead to resource consuming simulations. Though, these allow the determination of the influence of complex geometries on residual stresses and enable the simulation of following process simulations (e.g. bending or tensile tests).

The LSP process simulation can be divided into two phases. The first phase is named laser-pulse-phase and includes the laser pulse simulation followed by all plastic deformation. The laser-pulse-phase is commonly simulated using an explicit solver due to the high dynamic short time events. The second phase (relaxation-phase) includes the dynamic relaxation of the system, where the material reaches static-equilibrium. The stresses of the static-equilibrium are the residual stresses if no external forces are applied. In the relaxation-phase only elastic deformations occur. Some authors are using an explicit solver to calculate a state sufficiently close to the equilibrium. Peyre et al. (2007) used an explicit solver for the simulation of multiple laser impacts in a pure mechanical model. Thermal effects were considered in a second implicit simulation. The results of both, thermal and mechanical simulation were combined in a thermo-mechanical simulation to solve the coupled problem. Brockman et al. (2012) and Bhamare et al. (2013) added damping to the system during the explicitly solved relaxation-phase to reduce the computing time. Another possibility is the use of an implicit solver for the relaxation-phase to calculate the equilibrium as shown by Braisted and Brockman (1999). A third method is demonstrated by Achintha and Nowell (2011). Here, the plastic strains of an explicit analysis of the laser-pulse-phase were extracted and put into a second implicit analysis as eigenstrains to determine the resulting residual stress field. Most of the numerical discretisation techniques do not model the the vaporisation of the material. However, Fabbro et al. (1990) demonstrate an analytical one dimensional model to predict the pressure pulse based on a defined laser pulse.

Independently from the modelling technique, major challenges are the material behaviour at high strain rates and the simulation of the laser impact. Both, material behaviour and laser impact conditions are often not precisely known and very difficult to determine experimentally. These uncertainties make the validation of simulations by experiments more difficult.

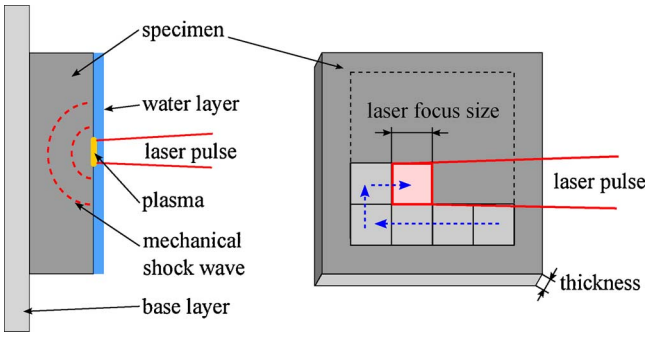

Fig. 1. Schematic of the LSP-process. The pulse leads by vaporization of the material to a plasma below the water layer which introduces shock waves into the material which lead to a characteristic residual stress field. The laser pulses are applied in a specific pattern.

This work is focused on the determination of the influence of tempering condition, material thickness, base layer, focus size and laser power density on the residual stresses in AA2198. Firstly, experimental results based on hole drilling measurements of the residual stresses are presented which are validated by X-ray diffraction. These results are used to set up a FE model which fits well to the measured data. Finally, comparisons between experiment and simulation for different temper conditions and focuses are shown.

2. Experimental techniques

2.1. Laser shock peening

A schematic of the LSP process is shown in Fig. 1. The first layer of the material is vaporized and turned into plasma by a pulsed laser. This high energy input leads to thermal expansion of the plasma which induces pressure shock waves propagating into the material. These shock waves lead to local plastic deformations close to the surface which cause residual stresses. The efficiency of the process is increased by transparent overlay, in this case a thin water film. The transparent overlay increases the duration and the maximum of the plasma pressure. In this work laser pulses were placed next to each other without overlap in the shown pattern.

LSP was performed at the Helmholtz–Zentrum Geesthacht with an Nd:YAG laser and a square laser focus with the focus size 1 mm or 3 mm. The laser pulse energy was varied between 0.6 J and 5 J with the Full Width at Half Maximum (FWHM) of 20 ns and a Gaussian profile. These laser pulse parameters lead to laser power densities between 2.78 GW/cm^2 and 25 GW/cm^2. The laser pulse energy and the FWHM are kept constant during the experiments. The experimental set-up is shown in Fig. 2. LSP specimens were fixed with a clamping device made of steel. To guarantee a laminar water film, water is sprayed above the area which will be peened. The material behind the specimen, the base layer, was varied during the experiments. It was investigated if the base layer affects the reflected shock wave. The superposition of reflected and initial shock waves could influence the resulting residual stress field. In this work three kinds of base layer were used, namely steel, air and a glued base layer.

Fig. 3 shows the used geometry of the specimens. The specimens dimensions are 90 mm/100 mm × 50 mm × 3.2 mm/4.8 mm. The investigated material is rolled AA2198 in T3 or T8 heat treatment condition. T3 condition was the delivery state of the material. Heat treatment to T8 condition was performed according to the material supplier

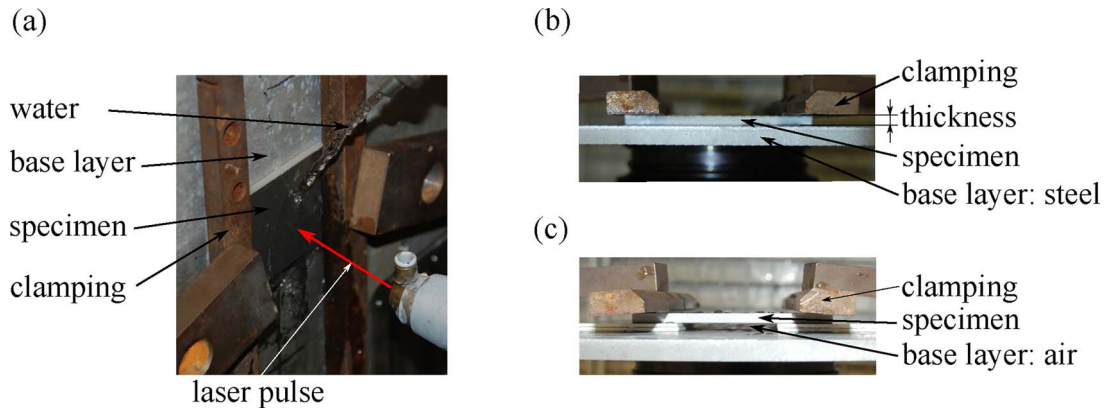

Fig. 2. (a) Experimental set-up of the LSP process. Side view of the base experiment with base layer steel (b) and air (c).

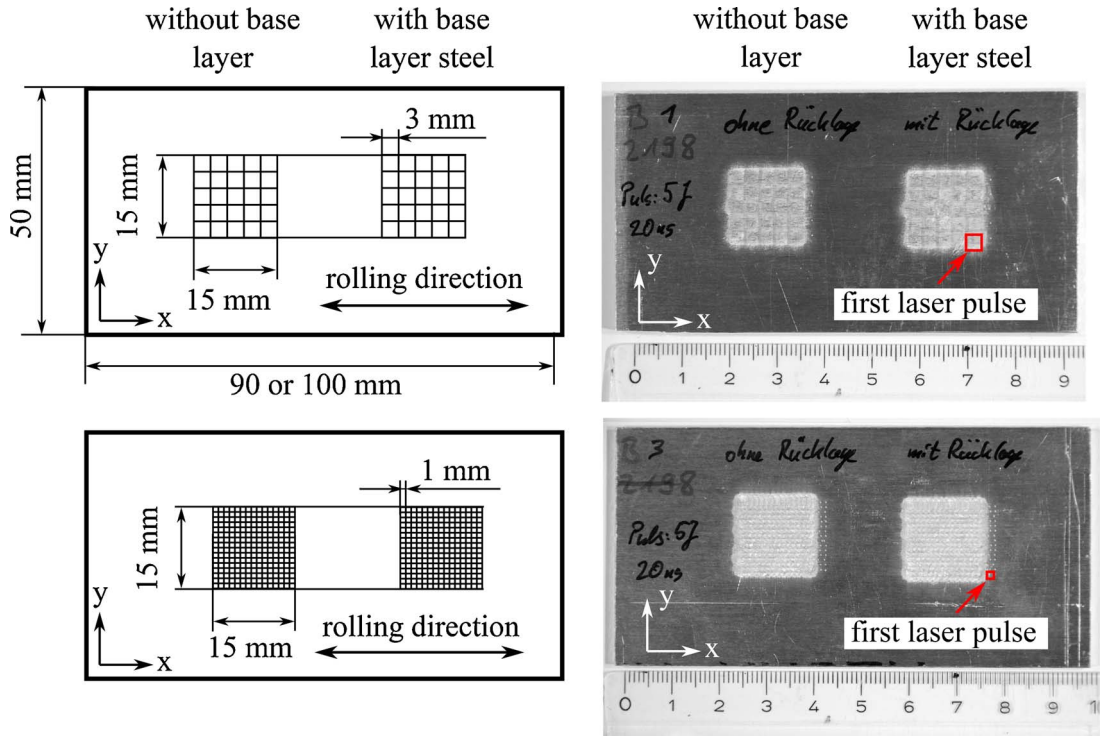

Fig. 3. Geometry of the peened specimens. Two areas of 15 mm × 15 mm were peened, one area without base layer (air) and the other with base layer steel.

specification (Constellium company).[1] Two areas (15 mm × 15 mm) on the surfaces of the specimens were peened. The right area was peened using as base layer steel. The left area was peened without base layer (base layer air). Depending on the focus size, 25 (3 mm laser focus) or 225 (1 mm laser focus) shots were needed to peen the area. The laser power density for a focus size 1 mm with a pulse energy 5 J (laser power density of 25 GW/cm^2) is significantly higher compared to a focus size 3 mm with pulse energy 5 J (2.78 GW/cm^2) or a focus size of 1 mm combined with the pulse energy 0.6 J (3 GW/cm^2), respectively. The sequence of the laser pulses is according to Fig. 1. The first laser pulse is marked in Fig. 3.

2.2. Incremental hole drilling method

Residual stresses were determined by the measurement system Prism from Stresstech. Prism is based on incremental hole drilling and electronic speckle pattern interferometry (ESPI) and can be summarized in three steps, see also Schajer (2010):

1. Drilling a hole incrementally.
2. Measurement of the surface deformation after each increment using ESPI.
3. Calculation of the residual stresses from surface deformations (Integral method).

During ESPI the surface around the hole is illuminated with coherent light. The reflection of the light leads to a phase shift for each pixel depending on the rough surface. The superposition of the reflected beam and a reference beam causes the speckle pattern. The intensity of each pixel depends on the phase shift after the reflection. Hence, the comparison of the pixel intensity before and after each hole increment indicates the movement of the pixel (Steinzig and Ponslet, 2003). The use of ESPI for the displacement measurement allows to consider the deformations of thousands of pixels. This amount of data enables a full field data analysis during the integral method. The relation between surface displacement of an arbitrary pixel and the residual stress can be

[1] To illustrate the effect of heat treatment, the mechanical properties are shown in Fig. 15.

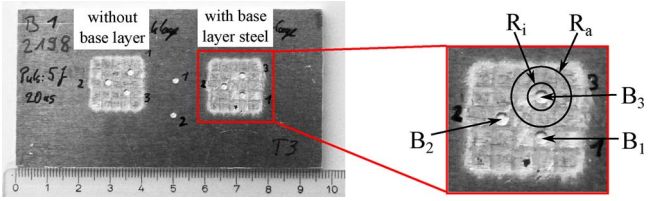

Fig. 4. Specimen after hole drilling measurement. The residual stresses in each peened area are measured by three measurements (e.g. B1, B2 and B3 in detailed view) and up to three measurements of the unpeened material for each used specimen. R_i and R_a indicate the circular ring in which surface displacements are considered during the residual stress calculation. The distance between the different holes is therefore large enough to prevent any influence from other drilled holes. The incremental hole drilling method assumed that the stresses within the circular ring are constant parallel to the surface.

obtained using the FE method. These relations between the measured displacement of each point at the surface and the residual stress components lead to an overdetermined system of equations which is solved by a full field least square technique (Ponslet and Steinzig, 2003a). The software tool of PRISM already includes the solution of these relations. Ponslet and Steinzig (2003b) summarize the assumptions and restrictions of the incremental hole drilling method using ESPI. For instance, incremental hole drilling applying the integral method assumes constant residual stresses parallel to the surface. Furthermore, in the integral method it is assumed that deformations are purely elastic. However, high residual stresses can lead to plastic deformation during the hole drilling. Chupakhin et al. (2016) have shown that plastic deformations occur when measuring LSP induced residual stresses approaching the material yield strength leading to errors in the residual stress determination. More recent, Chupakhin et al. (2017) have established a stress correction methodology based on an artificial neural network.

Fig. 4 shows the specimen after the application of the incremental hole drilling technique at eight positions. The holes were incrementally drilled with a diameter of 2 mm and a maximum depth of 1 mm. It is expected that residual stress gradients near the surface are higher than below the surface area. Therefore, drilling increments close to the surface have chosen to be smaller than below. The drilling increments are between 0.01 mm and 0.1 mm. The detailed view in Fig. 4 shows three holes (B_1, B_2 and B_3) in the laser shock peened area which are used for three residual stress measurements. The measured residual stress profiles do not indicate any influence of previous drilled holes. Hence, the distance between the holes is assumed to be large enough. The area in which pixels of the speckle pattern are considered is indicated by a circular ring, see Fig. 4, where R_i and R_a are the inner and outer radius, respectively.

3. Experimental results based on incremental hole drilling

3.1. Unpeened material

Residual stress measurement of the unpeened material of AA2198-T3 and AA2198-T8 for two specimen thicknesses of 3.2 mm and 4.8 mm are displayed in Fig. 5. These results represent the initial residual stress fields. The initial residual stresses are characterized by compressive stresses at the surface which are balanced with tensile stresses directly below this compressive region which decrease with depth. A slight anisotropy depending on the temper stage can be observed. The maximum stress in rolling direction (σ_{11}) for AA2198-T3 is higher than the maximum stress perpendicular to the rolling direction (σ_{22}). In contrast, the maximum stress in rolling direction for AA2198-T8 is lower compared to the stresses perpendicular to the rolling direction. Additionally, the penetration depth of the initial residual stresses is lower in AA2198-T8. The decreased penetration depth might be a result of the tempering which may lead to relaxations of the residual stresses.

3.2. Influence of the temper condition (T3 and T8)

Fig. 6 shows the residual stress distribution after LSP for the focus sizes of 3 mm and 1 mm in AA2198-T3 and AA2198-T8, specimen thickness 3.2 mm. A high ratio ($\sigma_{ii,max}/\sigma_Y > 0.8$) between maximum residual stress ($\sigma_{ii,max}$) and yield stress (σ_Y) may indicate an error of the determined residual stresses by the integral method due to the assumption of purely elastic deformation during the incremental hole drilling (Chupakhin et al., 2016). The correction method proposed by Chupakhin et al. (2017), based on a trained artificial network, contains the assumption of an equi-biaxial stress field. Therefore the residual stress measurements in Fig. 6(c) and (d) were corrected (σ_{cor}) based on the average value of σ_{11} and σ_{22}. At this point the developed correction method is not applicable for the experiments with 25 GW/cm^2 laser power density because of the non equi-biaxial stress field, see Fig. 6 (e) and (f). Therefore, these results have to be interpreted with care.

Comparing residual stress profiles with focus size 3 mm, it can be assessed that the residual stress profiles show similar patterns for both temper conditions. For both, residual stresses at the surface are tensile stresses. Residual stresses become compressive over the depth and reach a maximum at approximately 0.1 mm, afterwards the compressive residual stresses are decreasing and turn to tensile stresses again. The depth of the turning point from compressive to tensile stresses is the penetration depth.

While the maximum compressive stresses in AA2198-T3 and AA2198-T8 are equal, the penetration depth of the compressive stresses is different. The measurements indicate a higher penetration depth for AA2198-T3. Therefore, a steeper decrease of compressive residual stress can be observed for AA2198-T8. The higher penetration depth of AA2198-T3 is associated with the lower yield stress (approximately 310 MPa) compared to AA2198-T8 (approximately 447 MPa). The energy of the shock wave decreases depending on the passed distance inside the material. The energy of the pressure shock wave which is needed to cause plastic deformations depends on the yield strength of the material. Hence, in AA2198-T3 the energy of the shock wave at a higher penetration depth is still high enough to cause plastic deformations.

3.3. Influence of the focus size

The influence of the focus size is discussed based on the comparison of Fig. 6(a)–(d). For a nearly constant laser power density, 2.78 GW/cm^2 (focus size of 3 mm and pulse energy 5 J) and 3 GW/cm^2 (focus size of 1 mm and pulse energy 0.6 J), the experimental results show higher compressive residual stresses but a slightly lower penetration depth for the smaller focus size. The higher maximum stress can be caused by overlapping-effects of the plastically affected area of every laser pulse near the surface where the lower focus size may increase these overlapping-effects.

As mentioned before, AA2198-T3 and AA2198-T8 indicate tensile stresses at the surface for the focus size of 3 mm and the laser pulse energy of 5 J, see Fig. 6(a) and (b). This tensile stresses decreases with the reduction of the focus size, see Fig. 6(c) and (d)). But independent from the peening conditions, the residual stress profiles show a high slope at the surface. This slope and the tensile stresses might be caused by melting phenomena. Peyre et al. (1998) showed this effect for 55C1 steel and stated that the tensile stresses at the surface can be avoided with the use of an ablative overlay.

The higher penetration depth of a larger laser focus can be explained by the shock wave propagation depending on the focus size as described by Fabbro et al. (1998) for a circular laser focus at 55C1 steel. A smaller laser focus size leads to an increased energy loss of the shock wave during the wave propagation through the material due to the characteristic of a spherical wave front. A large laser focus leads to a planar wave front and loses less energy during the wave propagation compared to the spherical wave front at a small laser focus. Hence, the

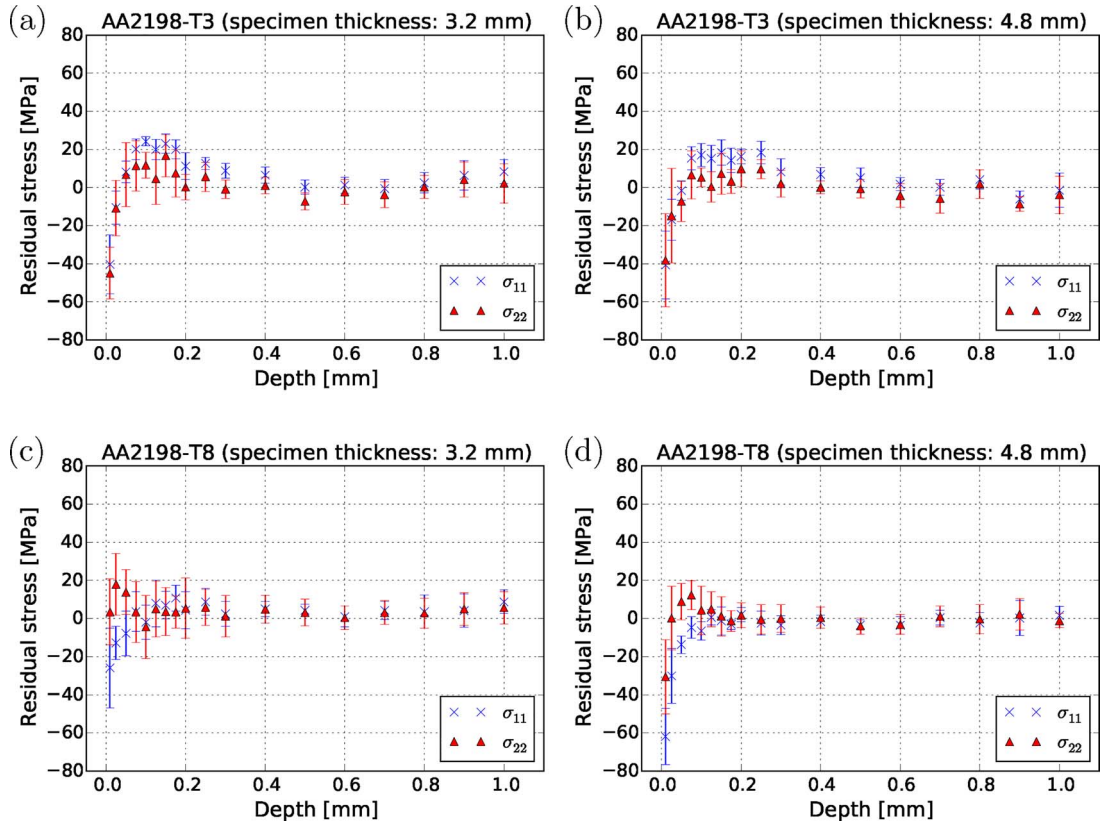

Fig. 5. Measured residual stress profiles over depth in the unpeened material AA2198-T3 and AA2198-T8 for two sheet thicknesses. The mean value with its standard deviation are shown. (a) AA2198-T3 with specimen thickness 3.2 mm; (b) AA2198-T3 with specimen thickness 4.8 mm; (c) AA2198-T8 with specimen thickness 3.2 mm; (d) AA2198-T8 with specimen thickness 4.8 mm.

lower penetration depth for the smaller focus size might be due to the higher energy loss of the shock wave.

3.4. Influence of the laser power density

A relative low laser power density of around 3 GW/cm^2 produces an approximately equi-biaxial residual stress field in specimens with 3.2 mm thickness as shown in Fig. 6(a)–(d). The reduction of the laser focus size to 1 mm while the pulse energy of 5 J is kept constant increases the laser power density up to 25 GW/cm^2. Berthe et al. (1998) showed the generation of breakdown plasma for a wavelength of 1.064 µm which is generated at laser power densities above 10 GW/cm^2. The breakdown plasma reduces the laser energy at the surface of the specimen. Whereas the pressure pulse scales according to the pulse energy at the surface of the specimen, shown by Berthe et al. (1999), the breakdown plasma can reduce the induced pressure pulse. However, the experimental results in Fig. 6(e) and (f) show a higher penetration depth of the compressive residual stresses compared to Fig. 6(c) and (d). This indicates, that the generated pressure pulse caused by the laser power density of 25 GW/cm^2 (focus size 1 mm; pulse energy: 5 J) is still higher than the pressure pulse resulting from the laser power density of 3 GW/cm^2 (focus size 1 mm; pulse energy: 0.6 J), additionally this leads to a non equi-biaxial residual stress field for both temper stages. However, as mentioned earlier, the results at this high laser power density have to be interpreted carefully, as the determined maximum stresses are close to the yield strength of the material.

In the following LSP-simulations, parameters were used which produces maximum compressive stresses below 80% of the yield stress to guarantee correct residual stress values.

3.5. Influence of the base layer

During the LSP-process mechanical shock waves are generated at the surface of the target. Depending on the energy loss of shock waves, reflected shock waves could influence the residual stress field. At the surface, laser generated shock waves are named primary shock waves and produce plastic deformations in the area next to the surface, see Fig. 7(a). During the shock wave propagation through the material the shock wave loses energy and the maximum pressure of the shock wave decreases. The shock wave might be reflected at the base layer, Fig. 7(b). The superposition of the reflected shock wave and stresses of the plastically deformed area at the surface or superposition with a new primary shock wave may cause additional plastic deformations. Hence, the resulting residual stress field might be influenced due to the shock wave reflection depending on the base layer material.

To observe a possible influence of the reflected shock wave the thinnest sheet thickness in this study (3.2 mm) and the highest laser power densities (25 GW/cm^2 at the focus size 1 mm and 2.78 GW/cm^2 at the focus size 3 mm) were investigated. These LSP-parameters produce the highest penetration depth of compressive residual stresses in this study, as shown in Fig. 6. Therefore, a maximum of the effect of the reflected shock wave is expected for these parameters. The base layers under investigation are a clamped steel plate and air. These base layers simulate typical cases during the practical application of the LSP-process. The resulting residual stress profiles for both temper conditions for both base layer versions are shown in Fig. 8. AA2198-T3 as well as AA2198-T8 show similar residual stress profiles for the base layer variation which only deviates in range of the measurement accuracy. Hence, it can be concluded, that the change of the applicable base layer (clamped steel plate or air) does not lead to a change of the residual stresses.

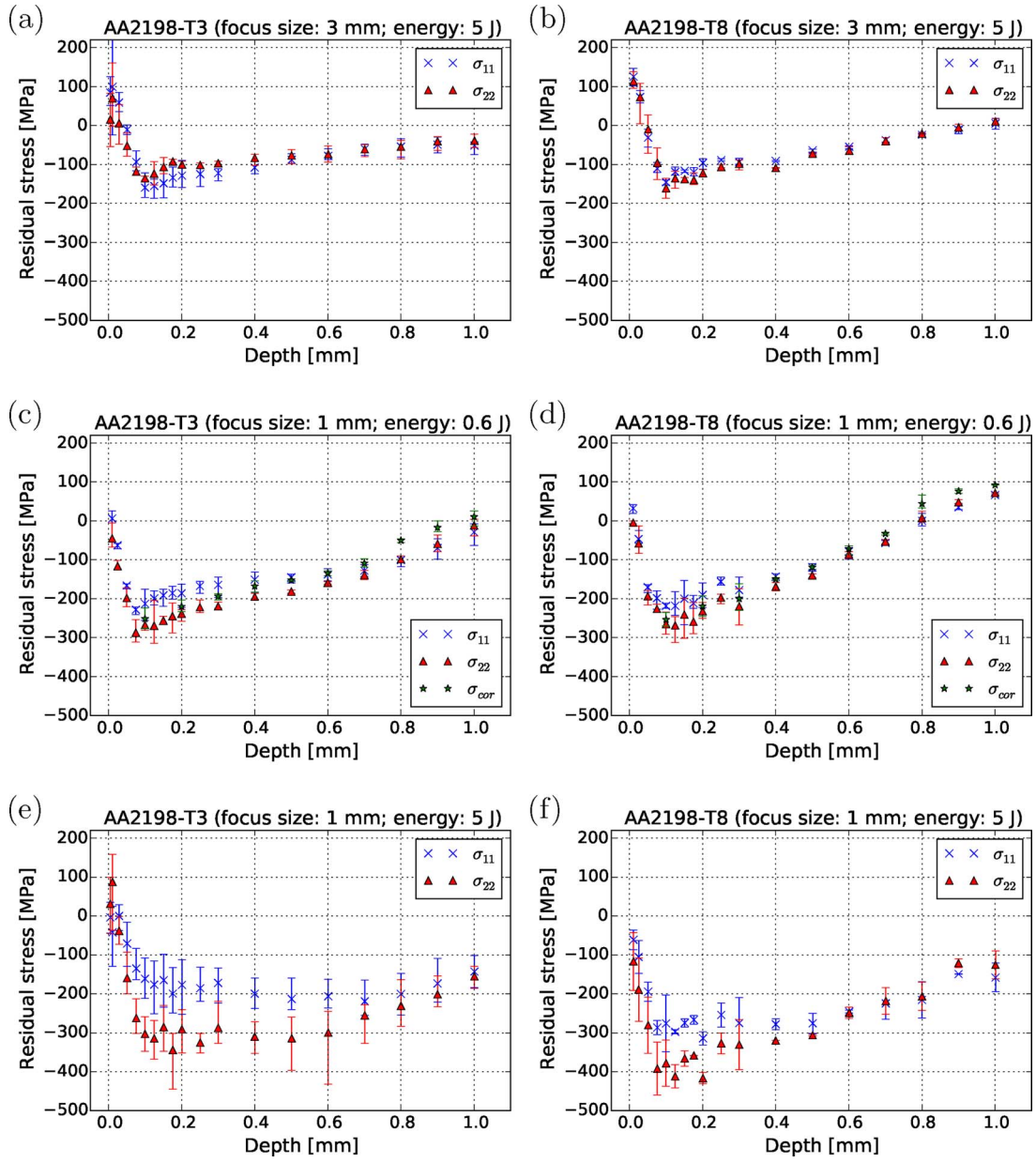

Fig. 6. Measured residual stress profiles after LSP in AA2198-T3 and AA2198-T8. While the base layer steel and the thickness of 3.2 mm were kept constant, the laser power density and the focus size vary between 2.78 GW/cm^2 and 25 GW/cm^2 and 3 mm and 1 mm, respectively. Due to the high maximum residual stresses close to the yield strength of the material, the measured results in of (c) and (d) are corrected using the method, proposed by Chupakhin et al. (2016). Due to the non equi-biaxial stress field, the results in (e) and (f) could not be corrected by this method. An increased laser power density leads to a higher penetration depth and higher maximum compressive stress. A decrease in focus size causes a lower penetration depth but higher maximum compressive residual stress.

However, the clamped steel plate might not provide enough contact for the complete transition of the shock wave. Therefore, a glued base layer consisting of AA2198 was used to improve the wave transition from the specimen to the base layer. The layer of glue is kept as thin as possible to minimize the influence of the glue on the wave propagation. Super glue and investment material were used as adhesive. The specimens consisting of AA2198-T3 with the thickness of 3.2 mm were treated with the focus size of 3 mm and the pulse energy of 5 J, Fig. 9(a), and with the focus size of 1 mm and the pulse energy of 5 J, Fig. 9(b). After the LSP-treatment, the specimens were released form

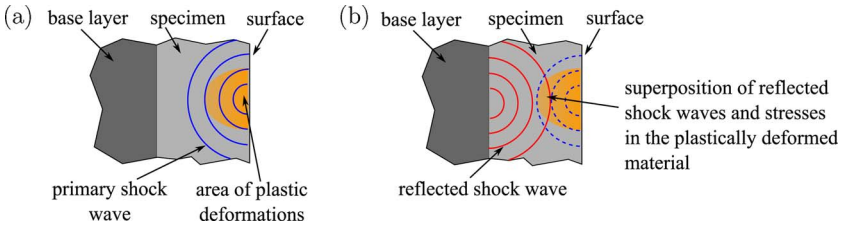

Fig. 7. Laser generated shock waves (primary shock wave) causes plastic deformations in the area next to the surface (a). Afterwards the superposition of reflected shock waves and stresses caused by plastic deformations of the primary shock wave may produce additional plastic deformations (b).

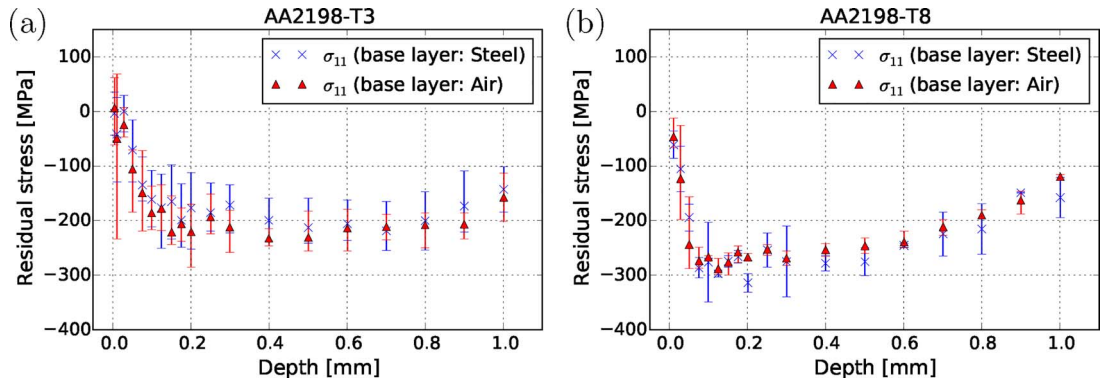

Fig. 8. Average value and maximum values of the measured residual stresses of laser peened AA2198-T3 (a) and AA2198-T8 (b) specimens with thickness of 3.2 mm and laser power density of 25 GW/cm^2 for two base layer variations (steel and air).

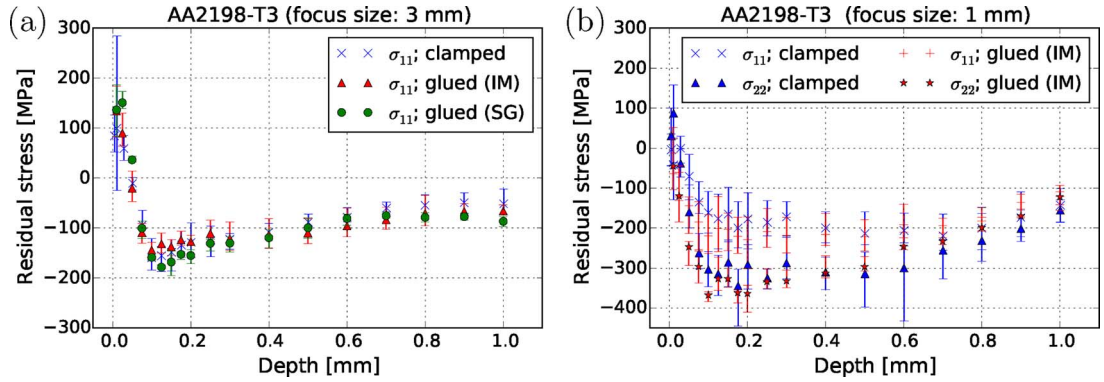

Fig. 9. Average and maximum values of the measured residual stresses of AA2198-T3 specimens (thickness: 3.2 mm) after LSP (pulse energy: 5 J; focus size: 3 mm (a) and size 1 mm (b)) for different base layers. As base layers, a clamped steel plate (clamped) and a glued AA2198 plate, where investment material (IM) and super glue was used as adhesive, are investigated. For the available process parameters and investigated material (AA2198 with sheet thickness of 3.2 mm) the measurements show no influence of the base layer material on the residual stress profile.

the base layer to guarantee the same measurement conditions during the incremental hole drilling method compared to the previous experiments. Considering the scatter of the measurements no significant influence of the glued base layers is observed. Based on these results it is assumed, that for the investigated process parameter range, the base layer does not have an impact on the resulting residual stresses of the AA2198 specimens which have at least a sheet thickness of 3.2 mm.

3.6. Influence of specimen thickness

Residual stress measurements of the unpeened material indicate an initial residual stress field slightly depending on the temper condition. The thickness could influences the residual stresses due to the position of the balancing tensile stresses even when the penetration depth of plastic strains is the same. In addition to different initial residual stresses, the thickness might affect the residual stress after LSP due to the influence of reflected shock waves at the base layer. The energy loss of reflected shock waves at the surface increases with increasing thickness of the specimens due to the extended distance between base layer and surface where LSP is applied. The LSP process is performed with the focus size of 3 mm and the base layer steel.

There is no significant difference between residual stresses after LSP of specimens with thicknesses of 3.2 mm and 4.8 mm detectable for AA2198-T3, Fig. 10(a). Considering the similar initial residual stresses of the AA2198-T3 specimens, Fig. 5, it is assumed that the reflected shock wave does not affect the residual stresses after LSP. Specimens of AA2198-T8 indicate slight differences depending on the thickness of the specimen, Fig. 10(b). However, the origin of these differences needs further investigation. Based on the previous experimental results the initial residual stresses and the shock wave reflection are not responsible for these differences.

3.7. Comparison of incremental hole drilling and X-ray diffraction

X-ray diffraction was used to determine residual stresses after LSP in AA2198-T3 and AA2198-T8 sheets. The diffraction measurements were performed at the P07B station of the HZG beamline HEMS (High Energy Materials Science), located in the PETRA III synchrotron radiation source at DESY (Deutsches Elektronen-Synchrotron, Germany). The photon energy was 87.1 keV, corresponding to a wavelength of 0.1429 Å. At this energy, complete diffraction rings can be recorded on a Perkin–Elmer area detector with a pixel size of 200 µm at a distance of 1570 mm from the specimen. Data reduction was performed using the program Fit2d (Hammersley, 1997). The scattering angle 2Θ of the Al (220) reflection was determined by fitting a Gaussian profile to the measured peaks. Strains were calculated from the shifts in the peak position. The residual stresses were calculated from the strains using the Young's modulus of $E = 78$ GPa and Poission's ratio of $\nu = 0.33$ for the Al(220)-reflection. For details on the residual stress analysis using diffraction, refer to the book of Fitzpatrick and Lodini (2003).

The geometry of the specimens for X-ray diffraction, Fig. 11(a), differs from the previews specimens. The width was reduced to 20 mm so that the X-ray beam can penetrate the whole width. The specimen thickness was 3.2 mm. A conical slit cell was used to define a gauge volume in the middle of the sample as shown by Staron et al. (2014). The gauge volume is defined by the cross-section of the X-ray beam of

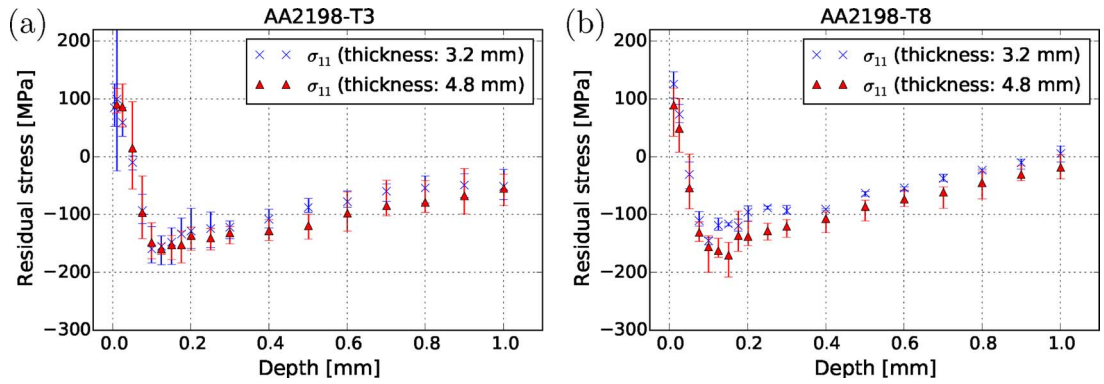

Fig. 10. Average and maximum values of the measured residual stresses of laser peened AA2198-T3 (a) and AA2198-T8 (b) specimens with base layer steel and laser power density of 2.78 GW/cm^2 for different specimen thicknesses 3.2 mm and 4.8 mm.

0.05 mm × 0.05 mm and the width of the conical slit of 0.02 mm. Together with the energy resolution given by the monochromator, the length of the gauge volume in beam direction is approximately 1.5 mm. With this set-up, a depth resolution (z-coordinate) given by the width of the X-ray beam of 0.05 mm is achieved while the extension of the gauge volume parallel to the sample surface is 0.05 mm × 1.5 mm ($x \times y$).

The lattice strains were determined in x and z- direction, Fig. 11(c). Because of the strong rolling texture of the AA2198 sheets the diffraction pattern does not show full rings but distinct intensity maxima, Fig. 12(a). Unfortunately, there is an intensity minimum in x-direction (horizontal). Therefore, an ellipse was fitted to the six intensity maxima to approximate 2Θ in x-direction, see Fig. 12(b).

The lattice spacing d_0 of the stress-free material was calculated assuming a plane stress state in the thin sample as well as equal strains in x and y-direction ($\varepsilon_{11} = \varepsilon_{22}$). d_0 was calculated for the unpeened material and in the laser treated area for every measured depth. In both cases, d_0 at the surface differs from d_0 inside the sheet. LSP could influence d_0 because of heat input or melting at the surface. However, the assumption of a plane stress state at the surface is surely valid. $d_0(z = 0)$ at the surface is used to calculate the residual stress at the surface. Inside the sheet the average value of $d_0(z > 0)$ is used. However, the average value of d_0 inside the sheet of the peened area and d_0 of the unpeened material are nearly identical. Corresponding to the hole drilling results, the residual stress is assumed to be equi-biaxial (stresses in x and y-direction are identical).

In addition to X-ray diffraction, residual stresses in the same specimens were measured using the incremental hole drilling technique. Fig. 13 shows the comparison of both techniques where similar patterns are observed. Especially at the surface, X-ray diffraction measurements show tensile stresses as seen in the hole drilling measurements. However, compressive residual stresses measured by X-ray diffraction are slightly lower compared to the hole drilling measurements in AA2198-T3. Overall, the residual stress results from incremental hole drilling and X-ray diffraction after LSP process show a good agreement. Therefore, it can be assumed that the residual stresses determined by incremental hole drilling provide a valuable basis for the subsequent process simulation.

4. Process simulation

4.1. Finite element model

A finite element (FE) model to predict the residual stress field after LSP is set-up as shown in Fig. 14(a). For the simulation of the dynamic process of LSP, ABAQUS/Explicit (6.14) is used. After the dynamic analysis of the laser pulses, an implicit simulation step is added to calculate the static equilibrium of the LSP-process (ABAQUS/Standard (6.14)). The material is modelled as a square of 65 mm × 65 mm with the thickness of 4.8 mm with fixed boundary conditions at the sides. The FE model consists of around two million three-dimensional continuum elements with reduced integration (C3D8R). Corresponding to results in the experiments it is assumed that the base layer does not influence the residual stress field. Therefore, the interface between base layer and specimen is not modelled and the LSP-process model do not contain the base layer. Any possible vaporization and melting phenomena at the surface of the specimen are disregarded. Therefore, the relatively low initial residual stresses, which are lower than 20 MPa after the depth of 0.02 mm (see Fig. 5), were neglected as well for simplicity.

The impact of laser pulses were simulated with a pressure loading on the surface. After each pressure pulse an explicit relaxation phase takes place where the modelled specimen reaches nearly equilibrium. After the last pressure pulse, the residual stresses were calculated using an implicit static solver. While the pressure pulse duration is about 0.2 µs the duration of the relaxation phase is assumed as 5.8 µs. The FE model includes the simulation of nine pressure pulses, see Fig. 14. These pressure pulses were placed without overlap. The pattern of the laser pulses corresponds to the sequence of the laser pulses during the experiments with laser focus size of a.

The chosen element size at the surface in the peened area is

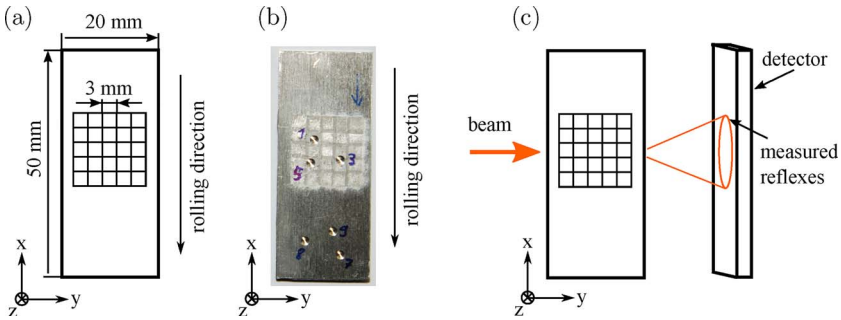

Fig. 11. (a) and (b) Geometry of the specimens which were used for the comparison between X-ray diffraction and hole drilling. (c) Beam direction during the X-ray diffraction measurement.

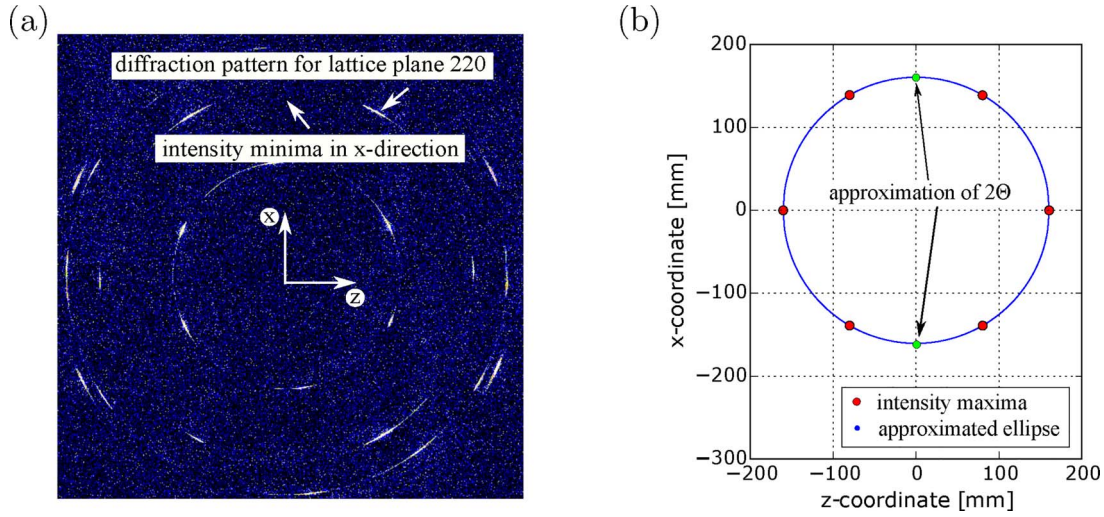

Fig. 12. (a) Diffraction pattern of AA2198. The intensity distribution along the rings is due to texture. (b) Ellipse fitted to the six intensity maxima of the (220) Debye–Scherrer ring.

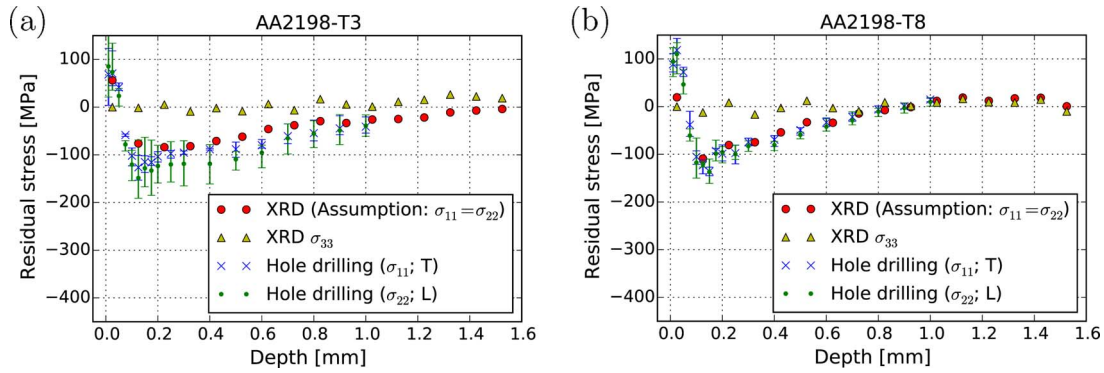

Fig. 13. Residual stresses of laser peened AA2198-T3 using the focus size 3 mm with pulse energy 5 J. Residual stresses measured by hole drilling compared to X-ray diffraction are in a good agreement.

relatively small (0.075 mm × 0.075 mm × 0.032 mm) to reach a mesh independent solution which was evaluated by a convergence study. To provide a cost efficient simulation, the element size in z-direction (depth) is smaller than in x and y-direction (parallel to the surface). The material behaviour was modelled as elastic-viscoplastic. The visco-plastic material modelling is based on the Johnson-Cook model (Johnson and Cook, 1983).

4.2. Constitutive model

During the LSP process high strain rates (up to 10^5–$10^7\,s^{-1}$) occur. Metals behave differently at that high strain rate compared to their quasi-static material behaviour. However, due to rate-dependent strain hardening and thermal softening because of heat generation during plastic deformation, this difference is often not exactly known (Amarchinta et al., 2010). An adequate and simple model to predict the material behaviour at high strain rates is the Johnson–Cook model. A number of the previously mentioned authors used the Johnson–Cook model in simulations of the LSP process (e.g. Sticchi et al., 2015; Spradlin et al., 2011 and Peyre et al., 2007). Amarchinta et al. (2010) compared different material models for the LSP simulation and concluded, that the Johnson-Cook model gives consistent results and is in better agreement with experiments compared to the other investigated material models. In the Johnson–Cook model, the yield stress

$$\sigma_Y = [A + B\cdot\varepsilon_P^n]\cdot\left[1 + C\cdot\ln\left(\frac{\dot{\varepsilon}_P}{\dot{\varepsilon}_{P,0}}\right)\right]\cdot[1 - (T^*)^m] \quad (1)$$

is a function of the equivalent plastic strain ε_P, the plastic strain rate $\dot{\varepsilon}_P$ and the homologous temperature T^*.[2] $\dot{\varepsilon}_{P,0}$ is the reference strain rate at the determination of the quasi-static material constants A (yield strength), B (strengthening coefficient), n (strain hardening exponent) and m (temperature dependency). C defines the influence of the strain rate on the yield stress. In this work, LSP is assumed to be a purely mechanical process. Therefore, the influence of the temperature is assumed to be negligible ($T^* = 0$). This assumption is for example also used by Sticchi et al. (2015) and Spradlin et al. (2011). However, some authors take thermal softening into account as Bhamare et al. (2013) and Peyre et al. (2007). Thermal softening reduces the yield stress and occurs due to the heat generation during plastic deformation. The strain rate dependency of the material at high strain rates, as present in the LSP process, is difficult to measure and not practicable in this work. Therefore, the dynamic strain hardening coefficient was approximated from the literature as $C = 0.01$ (Sticchi et al., 2015).

The quasi-static initial yield strength A and the strain hardening parameters B and n were identified from stress–strain curves of quasi-static tensile tests (see $\sigma_{T,1}$, $\sigma_{T,2}$, $\sigma_{L,1}$ and $\sigma_{L,2}$ in Fig. 15). The tensile tests were carried out corresponding to DIN EN 10002-1. Flat specimens with the thickness of 4.8 mm were tested at a strain rate $\dot{\varepsilon} = 1.8\cdot10^{-4}\,s^{-1}$. Fig. 15 shows the stress–strain curve of AA2198-T3 and AA2198-T8 for two loading directions (L: Longitudinal; T: Transversal to the rolling direction). According to Fig. 15, the elastic material behaviour is

[2] $T^* = \frac{T - T_r}{T_m - T_r}$, where T, T_r and T_m are the current temperature, the reference temperature and the melting temperature, respectively.

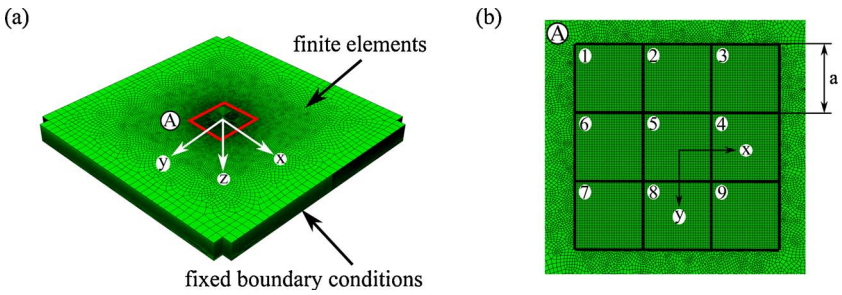

Fig. 14. Three-dimensional FE model for the simulation of the LSP-process. Pressure loading were used to simulate nine laser pulse impacts ((b) area 1–9) in the order of the laser pulse pattern of the experiments.

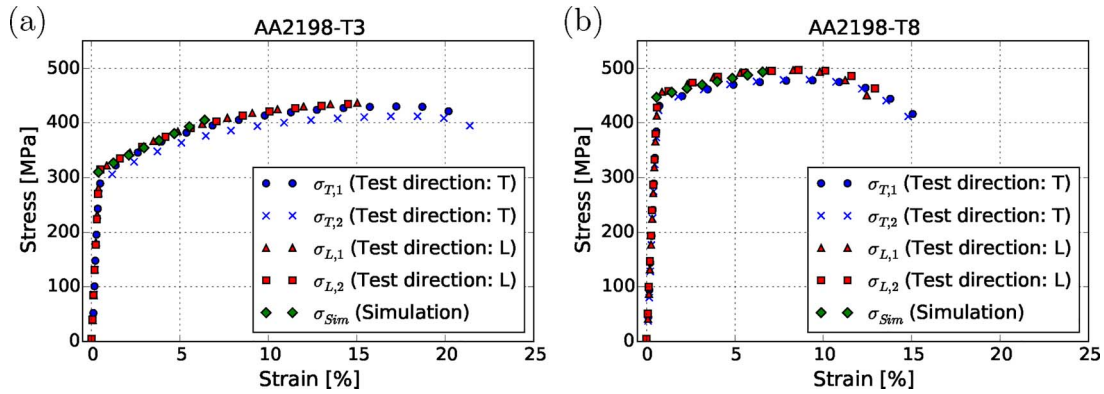

Fig. 15. Stress–strain curve of AA2198-T3 and AA2198-T8 using flat tensile tests (quasi-static strain rate). The measured plastic material behaviour is approximated using the Johnson–Cook model for the FE simulation (σ_{Sim}).

Table 1
Material parameters of AA2198-T3 and AA2198-T8. Most material parameters were determined by tensile tests shown in Fig. 15. Density ρ, Poisson's ratio ν and dynamic strain hardening coefficient C which are taken from literature (Sticchi et al., 2015).

	Parameter	Symbol	Value	Unit
AA2198-T3	Density	ρ	2.8	g/cm^3
	Young's modulus	E	78	GPa
	Poisson's ratio	ν	0.33	–
	Quasi-static yield strength	A	310	MPa
	Strengthening coefficient	B	1177	MPa
	Strain hardening exponent	n	0.894	–
	Dynamic strain hardening coefficient	C	0.01	–
AA2198-T8	Density	ρ	2.8	g/cm^3
	Young's modulus	E	78	GPa
	Poisson's ratio	ν	0.33	–
	Quasi-static yield strength	A	447	MPa
	Strengthening coefficient	B	484.3	MPa
	Strain hardening exponent	n	0.835	–
	Dynamic strain hardening coefficient	C	0.01	–

isotropic. The temper state significantly influences the yield strength which is higher for AA2198-T8 compared to AA2198-T3. The elastic material behaviour is independent from the tempering.

As the experimental tensile tests show only a slight material anisotropy and the use of a laser power density of 3 GW/cm^2 led experimentally to an approximately equi-biaxial residual stress field, an isotropic material behaviour is assumed in the LSP simulations of AA2198. To define isotropic material parameters for the simulation, the yield stresses in transversal and longitudinal direction were averaged. However, the error from this averaging is less than 5%. The strain hardening parameters B and n were identified to be in between the determined experimental hardening curves from transverse and longitudinal direction up to 5% plastic strain, see σ_{Sim} in Fig. 15. Material parameters used in this work are summarized in Table 1.

4.3. Laser pulse modelling

Laser pulses were modelled as pressure loading acting on the surface of the specimen. The real pressure pulse $p(x, y, t)$ is a function of time t and surface coordinates x and y. The determination of a valid function $p(x, y, t)$ for specific LSP process conditions is one of the major challenges in LSP simulations. LSP process parameters such as laser pulse power, laser pulse duration and transparent overlay have a strong influence on the resulting pressure pulse. This work presents an approach to estimate p based on simulated and measured residual stress fields.

As a square focus with a uniform laser density distribution is used, it is assumed that the pressure pulse does not depend on the surface coordinates x and y. Hence, the pressure pulse is uniform for the applied focus area and therefore constant in space, i.e. $p(t)$. The assumption of a space independent pressure were used in the early LSP simulation of Braisted and Brockman (1999) and were adopted by following simulations such as Peyre et al. (2007). The assumption of a constant pressure reduces the number of pressure pulse parameters which have to be adjusted. Additionally, the incremental hole drilling method does not allow a detailed spatial evaluation of the residual stresses parallel to the surface. Thus, the pulse adjustment using a space independent pressure pulse can be interpreted as the correlation between the in space averaged pressure pulse and the parallel to the surface averaged residual stresses. However, some authors used space dependant pressure pulse functions as well. Warren et al. (2008) showed the influence of laser pulse parameters on the resulting residual stresses using a spatial and temporal depending pressure pulse $p(x, y, t)$. The spatial distribution of the pressure corresponds to a Gaussian profile for a circular laser focus.

The shape of $p(t)$ is assumed to have the generic shape as shown in Fig. 16(a). Therefore, the determination of $p(t)$ requires the adjustment of only three independent parameters, t_I, t_{II} and p_{max}. t_I is the pressure pulse duration and t_{II} is the time when the maximum pressure p_{max} occurs. Residual stress profiles after LSP can be characterized by three parameters: the maximum compressive stress $\overline{\sigma}_{11,\mathrm{mps}}$, the depth z_{mps} at which $\overline{\sigma}_{11,\mathrm{mps}}$ occurs and the penetration depth of compressive residual

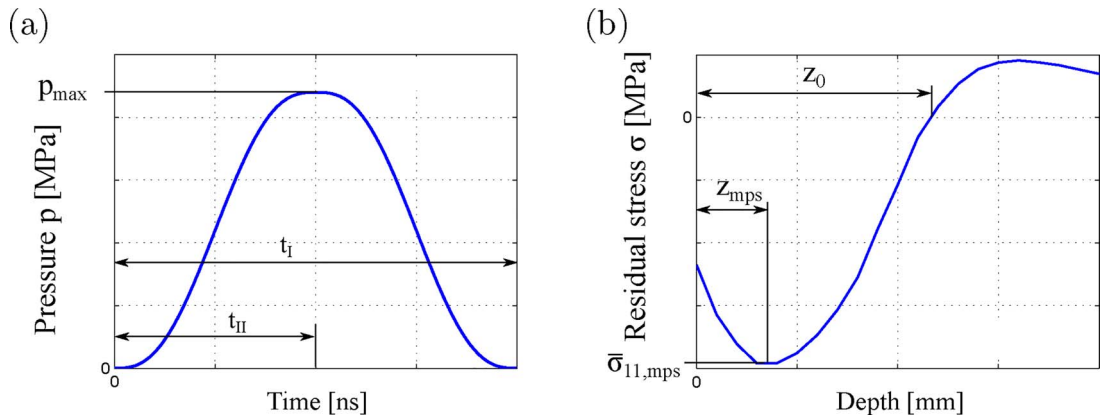

Fig. 16. (a) Characterization of the pressure pulse $p(t)$ by the pressure pulse duration t_I, the maximum pressure p_{max}, the time t_{II} at p_{max} and (b) the residual stress field characterized by the maximum residual stress $\bar{\sigma}_{11,\mathrm{mps}}$, the depth z_{mps} where $\bar{\sigma}_{11,\mathrm{mps}}$ occurs and the penetration depth z_0 where the residual stresses turn to tensile stresses.

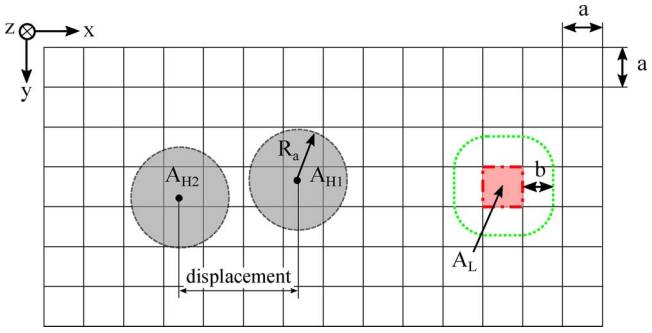

Fig. 17. Schematic of a peened area with the laser focus size a. Area A_{H1} and A_{H2} indicate the area where residual stresses parallel to the surface are assumed to be constant during the incremental hole drilling method. A_L is the area of one laser shot and b characterises the area where residual stresses are initiated caused by one laser pulse next to area A_L.

stresses z_0. Simulated residual stress profiles were fitted to the measured residual stress profiles by varying the pressure pulse parameters.

4.4. Stress averaging

FE simulations deliver complex three-dimensional residual stress fields. In particular, at the surface the simulations indicate a high variational spatial distribution of residual stresses, see Fig. 19. In contrast, the results of the hole drilling method are based on the assumption of constant residual stresses parallel to the surface in a defined area. This area is named A_H and is illustrated in Fig. 17 by a circle (dashed line) with the radius R_a. Because of the assumption of constant residual stresses it is not possible to experimentally measure the spatial in plane variation of residual stresses caused by LSP using the incremental hole drilling method. In the following an averaging scheme is proposed, which enables the comparison of measured and simulated residual stresses.

In order to compare simulated and measured residual stress fields, it is necessary to define an equivalent stress $\sigma_{ii,equ}$ of the simulated residual stress field (where index i defines the stress component; $i = 1, 2$). The calculation of an equivalent stress reduces the complex residual stress field $\sigma_{ii}(x, y, z)$ to an equivalent $\sigma_{ii,equ}(z)$ only depending on the z-direction. It is assumed, that the experimentally measured residual stress $\sigma_{M,ii}(z_k)$ corresponds to the average value in area A_H at the depth z_k. The displacement of the area may lead to slight variations of the measured residual stresses due to the fluctuations of the stress parallel to the surface, A_{H1} and A_{H2} see Fig. 17. Due to this only slight dependency on the measurement position and measurement inaccuracies, the average value $\bar{\sigma}_M(z_k)$ of several measurements at different location of the same residual stress field is considered as follows

$$\bar{\sigma}_M(z_k) = \frac{1}{N_m} \sum_{m=1}^{N_m} \sigma_{M,m}(z_k) \quad . \tag{2}$$

z_k is the depth of the k^{th} increment and $\sigma_{M,m}(z_k)$ is the measured residual stress of the m^{th} measurement. This average value corresponds to the average value $\bar{\sigma}(z)$ of the residual stress field at depth z_k neglecting edge-effects of the peened area ($\bar{\sigma}(z_k) \approx \bar{\sigma}_M(z_k)$). Edge-effects can be neglected, because measurements were in a sufficient distance to the borders of the peened area. Brockman et al. (2012) also used the average value of the residual stresses in a defined area to compare simulated residual stresses and measured residual stresses using X-ray diffraction.

Aiming on a cost efficient prediction of residual stresses in the simulation, the number of laser pulses which have to be simulated to calculate $\sigma_{ii,equ}(z)$ should be decreased to a minimum. Therefore it is assumed that the surface can be divided into a radiated area A_L (dash-dotted line) and an affected but not radiated area (dotted line), after each laser pulse, shown in Fig. 17. It is assumed that the affected but not radiated area, below which residual stresses are generated due to one laser pulse, can be characterized with an additional length b. Therefore, laser pulses outside the marked area (dotted line) do not influence the residual stress below the marked area A_L (dash-dotted line).

For the used laser process parameters it will be shown (see Section 4.5), that the laser pulse has only a short range effect, leading to the assumption $b < a$. In the following 3×3 laser pulses are considered to be sufficient. The residual stresses below the area of the centred laser pulse is not influenced by additional laser pulses outside this square of 3×3 laser pulses. Assuming periodicity of the residual stress field, the equivalent stress can be calculated by averaging the residual stresses within the area of the centred laser pulse as

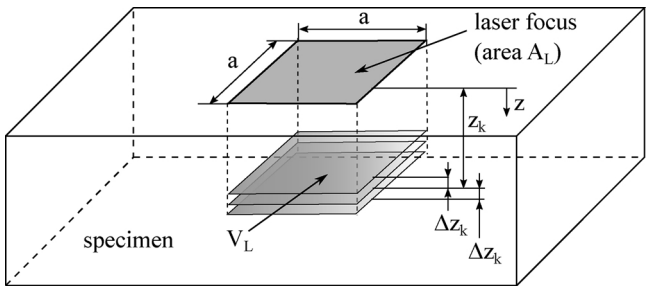

Fig. 18. Proposed stress averaging scheme for comparison of simulated to experimental measured residual stresses. Nodal stresses in the simulation are averaged within the volume V_L at a depth z_k to determine average residual stress over depth curve which is comparable to experimental measurements.

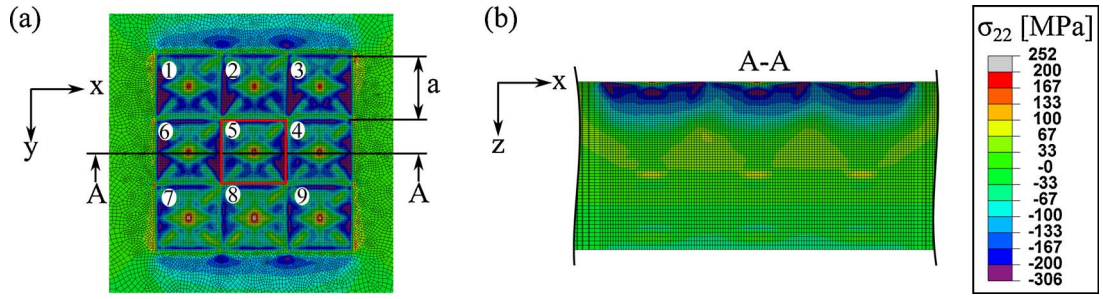

Fig. 19. LSP-simulation indicates high variations in residual stress field at the surface. For comparison with experiments the residual stresses were averaged in area 5 (marked area in (a)) according to the described stress averaging scheme. The stress pattern in x-direction looks similar to the shown stresses in y-direction after a rotation by 90° and results in the same stress prediction after the averaging scheme.

$$\sigma_{\mathrm{ii,equ}}(z_k) = \overline{\sigma}_{\mathrm{ii},A_L}(z_k) = \frac{1}{A_L}\int_{A_L} \sigma_{\mathrm{ii}}(x, y, z_k)\mathrm{dxdy}. \tag{3}$$

The applied averaging scheme is shown in Fig. 18. To calculate $\overline{\sigma}_{\mathrm{ii},A_L}(z_k)$, residual stresses at nodes[3] of the FE model were averaged during the post-processing. It is not ensured that nodes lie in the plain of A_L at depth z_k, therefore, A_L has to be shifted by Δz_k in positive and negative z-direction to span a volume V_L. For each depth z_k the residual stresses of all nodes within the volume V_L are averaged. V_L includes one to two layers of nodes, because of the relatively small Δz_k. Hence, the calculation of the averaged residual stresses $\overline{\sigma}_{\mathrm{ii}}$ at a depth z_k within the volume V_L corresponds to the area averaged residual stress $\overline{\sigma}_{\mathrm{ii},A_L}(z_k)$:

$$\sigma_{\mathrm{ii,equ}}(z) = \overline{\sigma}_{\mathrm{ii},A_L}(z_k) = \frac{1}{N_{V_L}}\sum_{n=1}^{N_{V_L}} \sigma_{\mathrm{ii},V_L,n}. \tag{4}$$

N_{V_L} is the number of all nodes in V_L. As a uniform mesh discretisation was used in the region of the laser pulses, the nodes are uniformly distributed in the volume, hence, the volume weights during the averaging can be neglected. This averaged stress value is used to define the standard deviation of the residual stress in V_L in terms of

$$S_{\mathrm{Sim}}(z_k) = \sqrt{\frac{1}{N_{V_L}}\sum_{n=1}^{N_{V_L}} (\sigma_{\mathrm{ii},V_L,n} - \overline{\sigma}_{\mathrm{ii},A_L})^2}\,. \tag{5}$$

The area in which residual stresses have to be calculated to fulfil the periodicity assumption is named representative area. In general, the number of laser pulses which needs to be simulated to calculate stresses within the representative area depends on focus size a and length of affected area b and may differ substantially based on the laser parameters and the investigated material. Additionally, b may vary because of residual stresses and strain hardening due to previous laser pulses.

4.5. Simulation results and discussion

At first, pressure pulse parameters were adjusted for a laser focus size of 3 mm and the laser pulse power of 5 J. The adjustment was done by using experimental results of the hole drilling method for AA2198-T3, see Section 2.2. The spatial residual stress distribution in the simulation after nine pressure pulses is shown in Fig. 19. For comparison with the experimental results, the residual stresses in the simulation are evaluated for the area of the 5th pressure pulse. A good agreement between measured and simulated residual stress is achieved by using the pressure pulse parameters: $p_{max} = 1350$ MPa, $t_I = 200$ ns and $t_{II} = 2$ ns, see Fig. 20(a).

Secondly, the condition ($a > b$) of the assumption of the nine shot model using the adjusted pressure pulse parameters was checked. Therefore, the averaged residual stress of the first pressure pulse area A_1 was determined after different laser pulses, see Fig. 21. The residual stress significantly changes after the second pressure pulse ($\overline{\sigma}_{11,A1}(t_1, z) \neq \overline{\sigma}_{11,A1}(t_2, z)$), however, the influence of the third pressure pulse is negligible for this area ($\overline{\sigma}_{11,A1}(t_2, z) \approx \overline{\sigma}_{11,A1}(t_3, z)$). Therefore, the condition $a > b$ holds for the adjusted pressure pulse and the investigation of nine pressure pulses is enough for comparison with experiment.

Simulated and measured residual stress profiles show similar characteristic w.r.t. penetration depth and stress distribution over depth. Hole drilling and X-ray diffraction results indicate tensile stresses at the surface, which are not reproduced by the simulation. As LSP was performed without coating, this might induce some melting phenomena due to the plasma which could result in tensile stresses at the surface. Such phenomena were neglected in the simulation. Additionally, high standard deviations of the stresses at the surface indicate high fluctuations of the residual stresses. Therefore, the assumption of constant residual stresses at the surface of the hole drilling method is doubtful. Additionally, residual stress fluctuations have to be taken into account when placing the gauge volume in the specimen during X-ray diffraction. The origin of the tensile stresses and its fluctuations at the surface as well as its influence on the measurement are subject of future investigations.

The pressure pulse adjustment enables the simulation of LSP on AA2198-T3 specimens under specific LSP conditions. To validate the developed model including the pressure pulse, the process model is applied to a specimen consisting of AA2198-T8. The resulting residual stress profile is compared to experiments in Fig. 20(b). Simulated and measured residual stress profiles are in good agreement. The simulation correctly predicts a lower maximum compressive stress and a decreased penetration depth in AA2198-T8 compared to AA2198-T3 which agrees well with the experimental observations.

The shape of the adjusted pressure pulse were used to simulate LSP with the focus size of 1 mm and the pulse energy of 0.6 J. The maximum pressure p_{max} was scaled, assuming a proportionality between the maximum pressure and the laser power density, which leads to $p_{max} = 1456$ MPa. The result of these LSP-simulations are shown in Fig. 20(c) for AA2198-T3 and (d) for AA2198-T8. The experimentally measured residual stresses are corrected by the method, proposed by Chupakhin et al. (2016) and correspond to Fig. 6(c) and (d). The simulated residual stresses show similar patterns compared to the measured residual stresses. The LSP-simulation shows higher plastic strains at the surface for the 1 mm focus size compared to the simulations using the 3 mm focus size. This explains the higher residual stresses at the surface with the use of the 1 mm focus size. Additionally, the penetration depth of plastic strains is lower for the LSP-simulation with 1 mm focus size. This coincide with the observation reported in Fabbro et al. (1998), where a lower penetration depth for a smaller laser focus is found. The influence of the focus size on the penetration depth can be linked to the shock wave characteristics. A larger focus size produces more planar shock waves which lose less energy and lead to a larger penetration depth compared to a smaller focus size where more spherical waves are observed in the simulation. However, the focus size may influence the generation of the shock wave as well, which influences

[3] The residual stresses at the integration can be used as well.

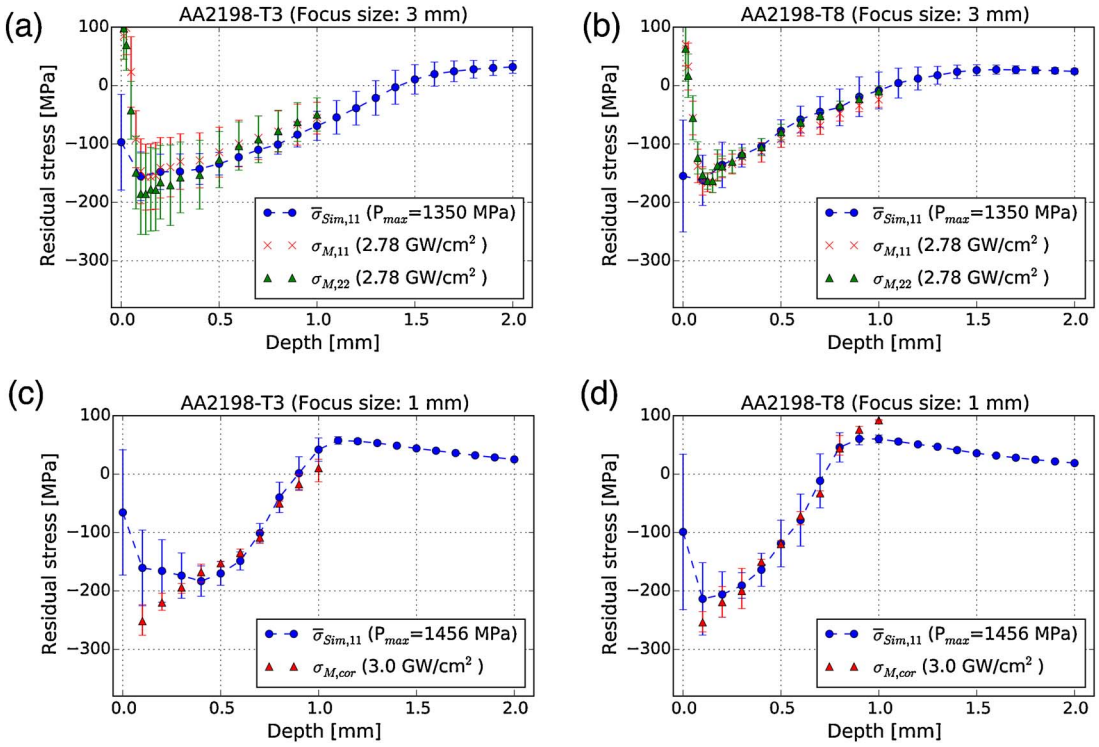

Fig. 20. Comparison between simulated ($\bar{\sigma}_{Sim,11}$) and measured ($\sigma_{M,11}$, $\sigma_{M,22}$ and $\sigma_{M,corr}$) residual stresses after LSP. for different focus sizes at a nearly constant laser energy density for both temper stages. The specimen thickness is 4.8 mm. $\bar{\sigma}_{Sim,11}$ shows always the standard deviation of the stresses which are taking into account during the averaging-scheme. (a) Pressure pulse parameters were adjusted for the LSP Simulation of AA2198-T3. Measured and simulated residual stresses after LSP are in good agreement. (b) The adjusted pressure pulse parameters were used to simulate LSP for AA2198-T8. The comparison between measured and simulated residual stress fields shows the validity of the applied pressure pulse as a lower maximum and penetration depth is correctly reproduced by the simulation. (c), (d) The adjusted pressure pulse was used for LSP-simulations with 1 mm focus size. Due to the high residual stresses, the experimental results were corrected, see Fig. 5(c) and (d). The maximum pressure is scaled according to the assumption of the proportionality between laser power density and maximum pressure. Measured and simulated residual stresses are in good agreement.

the shape of the pressure pulse. This influence is not considered during the LSP-simulations using the focus size of 1 mm and might be the reason for small differences of the measured and simulated residual stress profiles.

The shown LSP process model enables the prediction of residual stresses for different material properties. In future work, this model can be used to investigate the influence of LSP process parameters like overlap or the spatial distribution of the pressure pulse. Additionally, the influence of the material anisotropy will be investigated. This LSP process model could be used to study physical phenomena which are hard to measure e.g. the shock wave propagation and the plastically affected area of a single laser pulse.

5. Conclusion

The objective of this study is the experimental and simulative study of laser induced residual stresses of AA2198 sheets (thickness: 3.2 mm and 4.8 mm). Initial experimental investigations determine the influence of tempering (T3 and T8), base layer, specimen thickness, focus size and laser power density on the resulting residual stress field. Residual stress measurements using hole drilling were validated through measurements by X-ray diffraction. Afterwards these experimental results were used to set up a FE process model including suitable assumptions to adjust the present laser pressure pulse. Therefore, an appropriate comparative method for the spatial distribution of the residual stresses is proposed. The main conclusions of this work can be summarized as follows:

- Tempering of AA2198 influences the residual stress field significantly. Higher yield strength and different strain hardening behaviour lead to a lower penetration depth of compressive residual stresses for AA2198-T8 compared to AA2198-T3.
- The use of a low laser power density lead to equi-biaxial residual stresses. An increase of the laser power density causes non equi-

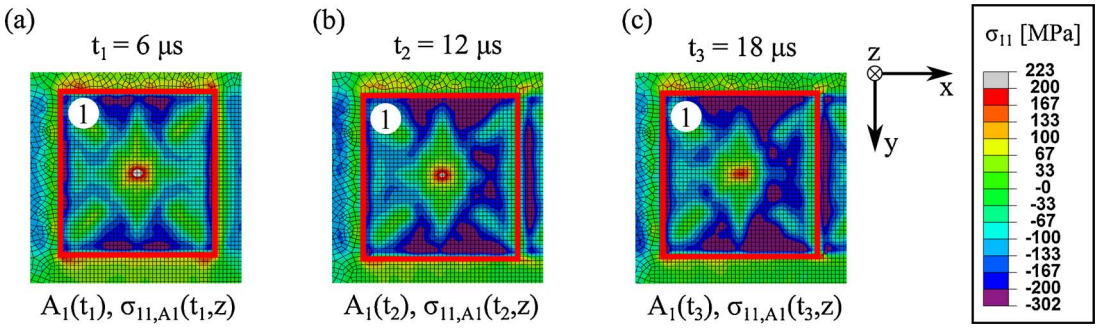

Fig. 21. Area of the first pressure pulse A_1 and the stress σ_{11} after the first pressure pulse (a), after the second pressure pulse (b) and after the third pressure pulse (c).

biaxial residual stresses. At a high laser power density the maximum compressive residual stress is limited by the yield strength. Therefore, higher compressive residual stress are achievable for AA2198-T8.

- The laser focus size influences the residual stress field significantly. A small laser focus leads to higher compressive residual stresses at the surface. Additionally, our experiments indicate a lower penetration depth of compressive residual stresses for a small focus size, which agrees well with results in the literature (Fabbro et al., 1998).
- The considered thickness of 3.2 mm and 4.8 mm as well as the base layer do not influence the residual stress field after LSP. Air and a clamped steel plate were considered as base layer for practical applications. Additionally, a glued base layer was used to study the effect of the reflected shock wave. The experiments do not indicate an influence of the base layer on the residual stresses. Hence, it is assumed, that the reflected shock wave do not lead to additional plastic deformations.
- Simulation results indicate residual stress fields with large spatial fluctuations. Therefore, assumptions of measuring methods must be reconsidered, e.g. the gauge volume during the X-ray diffraction has to be large enough. Stress averaging in the simulation enables the comparison between measured and simulated residual stress fields. For low laser power density it is sufficient to simulate a pattern of 3×3 laser pulses. A higher laser power density or a lower yield stress could lead to an increased plastically influenced area for each laser pulse. Thus, the use of nine pressure pulses to produce an representative residual stress field has to be checked for other process conditions.
- A suitable pressure pulse for a Gaussian shaped laser pulse with the FWHM of 20 ns and the total energy of 5 J was adjusted for AA2198-T3. For purpose of validation, the adjusted pressure pulse was used to simulate LSP on materials of different temper stages and for different focus sizes. The results show a very good agreement. The LSP process model enables the prediction of laser induced residual stresses for different material properties.

Acknowledgements

We acknowledge Deutsches Elektronen-Synchroton (DESY), Germany, for using synchrotron radiation at beamline P07B of Helmholtz-Zentrum Geesthacht. The authors would like to thank R. Dinse for the preparation of the specimens.

References

Achintha, M., Nowell, D., 2011. Eigenstrain modelling of residual stresses generated by laser shock peening. J. Mater. Process. Technol. 211, 1091–1101.
Amarchinta, H.K., Grandhi, R.V., Clauer, A.H., Langer, K., Stargel, D.S., 2010. Simulation of residual stress induced by a laser peening process through inverse optimization of material models. J. Mater. Process. Technol. 210, 1997–2006.
Askar'yan, G., Moroz, E., 1963. Pressure on evaporation of matter in a radiation beam. Soviet J. Exp. Theor. Phys. 16, 1638.
Berthe, L., Fabbro, R., Peyre, P., Bartnicki, E., 1998. Experimental study of the transmission of breakdown plasma generated during laser shock processing. Eur. Phys. J. Appl. Phys. 3, 215–218.
Berthe, L., Fabbro, R., Peyre, P., Bartnicki, E., 1999. Wavelength dependent of laser shock-wave generation in the water-confinement regime. J. Appl. Phys. 85, 7552–7555.
Bhamare, S., Ramakrishnan, G., Mannava, S.R., Langer, K., Vasudevan, V.K., Qian, D., 2013. Simulation-based optimization of laser shock peening process for improved bending fatigue life of Ti-6Al-2Sn-4Zr-2Mo alloy. Surf. Coat. Technol. 232, 464–474.
Braisted, W., Brockman, R., 1999. Finite element simulation of laser shock peening. Int. J. Fatigue 21, 719–724.
Brockman, R.A., Braisted, W.R., Olson, S.E., Tenaglia, R.D., Clauer, A.H., Langer, K., Shepard, M.J., 2012. Prediction and characterization of residual stresses from laser shock peening. Int. J. Fatigue 36, 96–108.
Chupakhin, S., Kashaev, N., Huber, N., 2016. Effect of elasto-plastic material behaviour on determination of residual stress profiles using the hole drilling method. J. Strain Anal. Eng. Des. 51, 572–581.
Chupakhin, S., Kashaev, N., Klusemann, B., Huber, N., 2017. Artificial neural network for correction of effects of plasticity in equibiaxial residual stress profiles measured by hole drilling. J. Strain Anal. Eng. Des. 52, 137–151.
Clauer, A.H., Fairand, B.P., Slater, J.E., 1977. Laser shocking of 2024 and 7075 aluminum alloys. Technical Report. Battelle Columbus Labs, OH, United States.
Clauer, A.H., Lahrman, D.F., 2001. Laser shock processing as a surface enhancement process. Key Eng. Mater. 197, 121–144.
Ding, K., Ye, L., 2006. Simulation of multiple laser shock peening of a 35CD4 steel alloy. J. Mater. Process. Technol. 178, 162–169.
Dursun, T., Soutis, C., 2014. Recent developments in advanced aircraft aluminium alloys. Mater. Des. 56, 862–871.
Fabbro, R., Fournier, J., Ballard, P., Devaux, D., Virmont, J., 1990. Physical study of laser-produced plasma in confined geometry. J. Appl. Phys. 68, 775–784.
Fabbro, R., Peyre, P., Berthe, L., Scherpereel, X., 1998. Physics and applications of laser-shock processing. J. Laser Appl. 10, 265–279.
Fairand, B., Wilcox, B., Gallagher, W., Williams, D., 1972. Laser shock-induced microstructural and mechanical property changes in 7075 aluminum. J. Appl. Phys. 43, 3893–3895.
Fitzpatrick, M.E., Lodini, A., 2003. Analysis of Residual Stress by Diffraction Using Neutron and Synchrotron Radiation. Taylor & Francis.
Hammersley, A., 1997. Fit2d: An Introduction and Overview. European Synchrotron Radiation Facility Internal Report ESRF97HA02T 68.
Johnson, G.R., Cook, W.H., 1983. A constitutive model and data for metals subjected to large strains, high strain rates and high temperatures. In: Proceedings of the 7th International Symposium on Ballistics. The Hague, The Netherlands. pp. 541–547.
Ocana, J.L., Morales, M., Molpeceres, C., Torres, J., 2004. Numerical simulation of surface deformation and residual stresses fields in laser shock processing experiments. Appl. Surf. Sci. 238, 242–248.
Peyre, P., Berthe, L., Scherpereel, X., Fabbro, R., 1998. Laser-shock processing of aluminium-coated 55c1 steel in water-confinement regime, characterization and application to high-cycle fatigue behaviour. J. Mater. Sci. 33, 1421–1429.
Peyre, P., Chaieb, I., Braham, C., 2007. FEM calculation of residual stresses induced by laser shock processing in stainless steels. Modell. Simul. Mater. Sci. Eng. 15, 205–221.
Peyre, P., Fabbro, R., Merrien, P., Lieurade, H., 1996. Laser shock processing of aluminium alloys. Application to high cycle fatigue behaviour. Mater. Sci. Eng. A 210, 102–113.
Ponslet, E., Steinzig, M., 2003a. Residual stress measurement using the hole drilling method and laser speckle interferometry. Exp. Tech. 27, 17–21.
Ponslet, E., Steinzig, M., 2003b. Residual stress measurement using the hole drilling method and laser speckle interferometry part III: analysis technique. Exp. Tech. 27, 45–48.
Reid, L., 2003. Sustaining an aging aircraft fleet with practical life enhancement methods. Technical Report. DTIC Document.
Schajer, G.S., 2010. Advances in hole-drilling residual stress measurements. Exp. Mech. 50, 159–168.
Spradlin, T.J., Grandhi, R.V., Langer, K., 2011. Experimental validation of simulated fatigue life estimates in laser-peened aluminum. Int. J. Struct. Integr. 2, 74–86.
Staron, P., Fischer, T., Keckes, J., Schratter, S., Hatzenbichler, T., Schell, N., Müller, M., Schreyer, A., 2014. Depth-resolved residual stress analysis with high-energy synchrotron X-rays using a conical slit cell. Mater. Sci. Forum 768–769, 72–75.
Steinzig, M., Ponslet, E., 2003. Residual stress measurement using the hole drilling method and laser speckle interferometry: Part 1. Exp. Tech. 27, 43–46.
Sticchi, M., Staron, P., Sano, Y., Meixer, M., Klaus, M., Rebelo-Kornmeier, J., Huber, N., Kashaev, N., 2015. A parametric study of laser spot size and coverage on the laser shock peening induced residual stress in thin aluminium samples. J. Eng. 1.
Warren, A., Guo, Y., Chen, S., 2008. Massive parallel laser shock peening: simulation, analysis, and validation. Int. J. Fatigue 30, 188–197.